Ultramicroscopy 123 (2012) 80–89

Contents lists available at SciVerse ScienceDirect

Ultramicroscopy

journal homepage: www.elsevier.com/locate/ultramic

Capturing the signature of single atoms with the tiny probe of a STEM ☆

C. Colliex [a,*], A. Gloter [a], K. March [a], C. Mory [a], O. Stéphan [a], K. Suenaga [b], M. Tencé [a]

[a] Laboratoire de Physique des Solides (UMR CNRS 8502), Bldg. 510, Université Paris Sud, 91405 Orsay, France
[b] Nanotube Research Centre, National Institute of Advanced Industrial Science and Technology, Tsukuba 305-8565, Japan

ARTICLE INFO

Available online 27 April 2012

Keywords:
Scanning transmission electron microscope (STEM)
Electron energy loss spectrometry (EELS)
Single atom identification

ABSTRACT

With their first scanning transmission electron microscope (STEM), Albert Crewe and his collaborators have succeeded 40 years ago in bringing to reality a dream for all electron microscopists, to see individual atoms. In the derivation of Crewe's pioneering work, the present review describes various historical and present steps, involving continuous instrumental and methodological developments as well as the preparation of suitable specimens. They have lead to the identification of individual atoms by electron energy-loss spectroscopy (EELS) and to the demonstration of atom-by-atom spectroscopy. Beyond these spectacular successes which open wide fields of use, most recent technical achievements, such as the introduction of monochromators on the incident electron beam or of optical spectrometers for recording spectra (in the visible as well as in the X-ray domain), will undoubtedly lead to refine the accessible signature of single atoms and molecules.

1. Introduction

During the *7th International Conference on Electron Microscopy (ICEM)* in 1970 at Grenoble, Albert Crewe delivered a speech in which he showed the first images of individual atoms recorded with a Scanning Transmission Electron Microscope (STEM) home-built in his laboratory in Chicago. This was a great experimental achievement which gained its well deserved success in the audience. Meanwhile in a paper published in Science [1], the authors pointed out the key ingredients in their study: (i) the visibility factor for single U and Th atoms deposited on a thin layer of carbon film was approximately demonstrated in the micrographs; (ii) the signal of the individual heavy atoms, clearly visible in the annular dark field image, could not be seen in the inelastic image; (iii) the heavy atoms were attached at preferential sites on given molecules, the distance between the involved pairs or chains of atoms in the micrographs were in satisfactory agreement with the predicted ones.

From these remarks, it was possible to draw immediate conclusions: (i) in these early experiments, the key of the success was the achievement of the required signal-to-noise and not of the required spatial resolution, the probe diameter was typically of 0.5 nm on the specimen surface while the specimen incorporated individual heavy atoms separated by more than 1 nm; (ii) consequently the preparation of a well-adapted specimen was a pre-requisite which could not be ignored; (iii) for the first time, simultaneous multi-detection schemes involving an ADF detector for elastic scattering and an EELS spectrometer to discriminate zero-loss and inelastic signals was employed. Practically, the other fundamental instrumental component was the cold field emission source of high brightness firing a high flux of electrons into a very narrow probe, so that the statistical noise of the supporting layer could remain below the level of the meaningful signal of the heavy atoms. This was the starting point on which the Chicago group developed extensive studies relying on the visibility of single atoms with improved spatial resolution [2]. In parallel, they introduced the *Z* contrast imaging mode as the ratio between the elastic and inelastic signals, independent of the support thickness fluctuations, to enhance the visibility of the heavy atoms.

During the following decade, several companies worked at developing commercial STEM instruments relying on the basic principles of the Chicago microscope, Vacuum Generators which had a long practice in high vacuum technologies being the only one to produce reliable machines. We had the chance in Orsay to acquire in 1980 one of them, a VG HB501 microscope, which is still in daily operation. The purpose of the present paper is to review how along these past three decades, the track of single atoms with tiny STEM probes has progressed to produce richer and richer signals, which open today new routes in quite diversified fields from nanotechnology to molecular biology.

☆ Note added in proof: after submission of the manuscript, we have become aware of the nearly simultaneous submission of two papers demonstrating the same achievement, i.e. "EDX spectroscopy on single atoms" and "Single atom identification by EDX", respectively by K. Suenaga et al. and by T.C. Lovejoy et al.

* Corresponding author.
E-mail address: christian.colliex@u-psud.fr (C. Colliex).

0304-3991/$ - see front matter © 2012 Elsevier B.V. All rights reserved.
http://dx.doi.org/10.1016/j.ultramic.2012.04.003

2. Instrumentation and methodology

As already pointed out, the basic principles of the STEM microscope are quite straightforward, following the original design by Crewe and coworkers [3] made of an electron gun, an electron spectrometer and electron detectors (see Fig. 1 which compares the global design of two STEM instruments published at a 40 year interval). A fine metallic tip delivers by a field emission process a beam of electrons accelerated typically at 30 to 200 kV and focused on the thin specimen into a probe, the characteristics of which (size, intensity, angular convergence) are essential to determine the quality of the recorded images. This is the incident probe. While traveling through the thin foil, the electrons suffer different scattering processes with the target and produce complementary signals carried by the transmitted beam (scattering angle distribution, energy-loss distribution) or in emitted signals (photons in quite broad spectral domains from the IR to the X-ray one or secondary electrons). The strategy then is to pick for each impinging electron, the signals (S_i) which it has generated while interacting with the target, and to reduce at the most, the number of those which do not carry information. This is achieved by implementing the best combination of detectors facing the specimen. In the early machine, the displacement of the probe on the specimen was realized by a simple analogically controlled electrostatic deflection system, while in the modern instruments a digital unit governs the probe scan and acquires, stores and processes all signals recorded in parallel for each probe position.

2.1. About the incident probe on the specimen

Cold field emission guns (CFEG) constitute the electron sources of highest brightness currently available on STEM microscopes. Furthermore, they exhibit a narrow intrinsic energy distribution typically between 0.3 and 0.4 eV, which offers clear advantages for high resolution EELS studies on one hand and for reducing the contribution of the chromatic aberration of the illumination optics on the other hand. For many years following the work by Crewe and coworkers, the simple design made of a [3 1 0] oriented W tip under high vacuum environment and followed by a double set of electrodes for extraction and acceleration has been commonly used on the VG microscopes. Very recently, new gun designs have been made available, Nion producing a gun of similar type but including an electrostatic lens to vary the divergence of the extracted beam before acceleration [4] and JEOL introducing a [1 1 1] W emitter with a nanotip [5]. It is interesting to point out that after a general trend to promote higher acceleration voltages between 100 and 200 kV, the move has reversed and new STEM instruments are preferentially dedicated to run at lower voltages (40 to 60 kV) in order to reduce beam damage induced by the extremely high doses of incident electrons (see below).

The focusing optics transferring the electrons from the source cross-over to the specimen has been revolutionized by the introduction of aberration correctors in the late nineties. In parallel with the work of Haider et al. who built a C_s corrector for a 200 kV CTEM [6,7] and then developed it for improved phase contrast imaging, Krivanek et al. concentrated their effort on

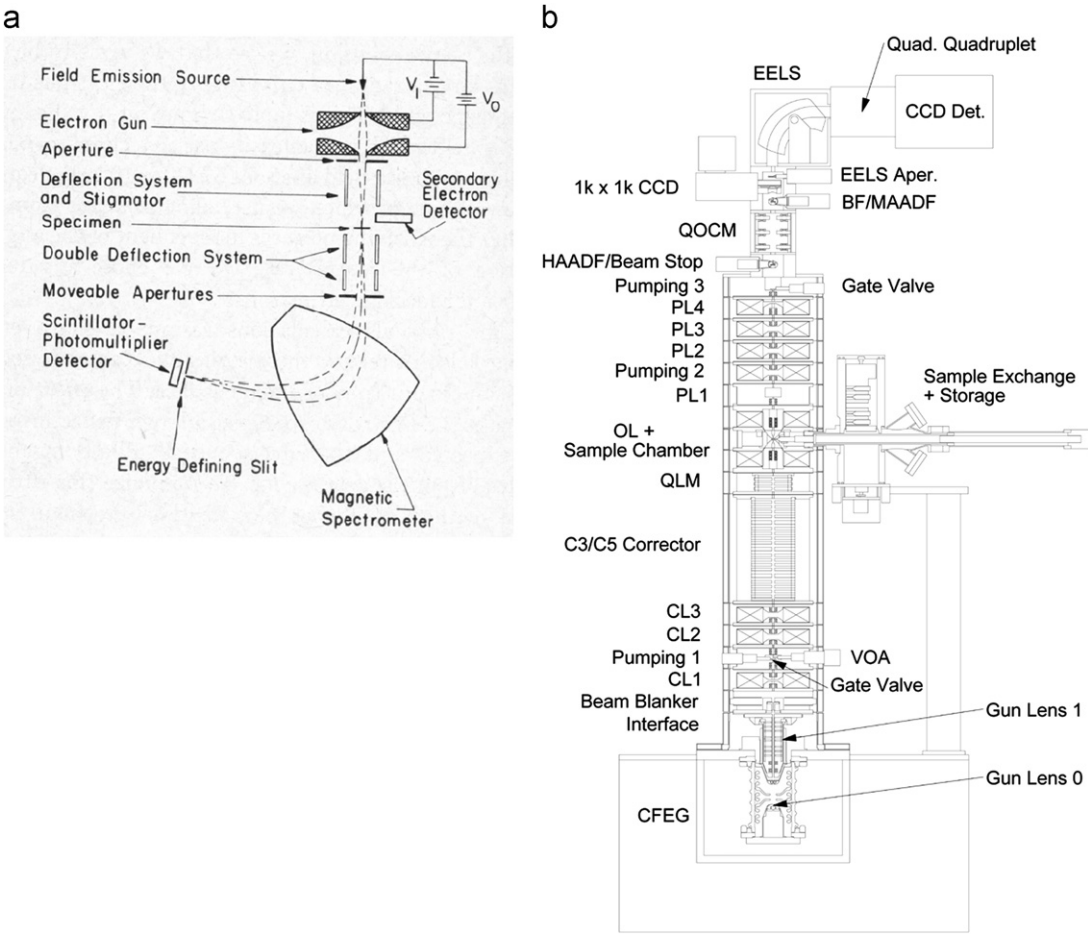

Fig. 1. Schematic design of the first STEM instrument built by A. Crewe and colleagues at Chicago in the sixties (left) compared to that of the latest generation of UltraSTEM machine built by Nion in 2010 (right), see respectively [3,4].

achieving C_s correction for probe forming lenses in a STEM configuration by using a combination of quadrupoles and octupoles. They paved the way to significant improvements both in attainable spatial resolution and in probe current within a given probe diameter, by constructing two generations of correctors for third order correction towards sub-Å electron beams [8], then for third and fifth order correction towards sub-0.5 Å electron beam [9]. Rapidly convinced that the targeted performance was very stringent for many other criteria, such as the level of mechanical and electric stabilities, the Nion team developed and built a completely new dedicated STEM instrument, the UltraSTEM at 100 and 200 kV (see [4,10,11] for extensive descriptions), the general design of which being shown in Fig. 1(b) for comparison with its Crewe's ancestor. The most recent machine, which has been installed in Orsay a few months ago, can operate at voltages from 200 kV down to 40 kV, reach a probe size <60 pm at 200 kV and $\sim$125 pm at 40 kV, or deliver a 1 nA current into a probe <150 pm at 200 kV [4]. For comparison with Crewe's first STEM which included no focusing lens, this new generation of microscope incorporates two gun lenses, three condenser lenses, a C3/C5 corrector and an objective lens between the source of electrons and the specimen.

Let us mention similar projects under active development aiming at similar goals. In Japan, the microscope built by the JEOL company for the tripleC project, corrects the spherical third order aberration and higher order astigmatism by a combination of three dodecapoles (the Delta corrector) together with C_c correction in the latest design [5,12,13]. The objective of this project is again to have a sub-Å probe at low voltages between 30 and 60 kV for studying very thin and beam sensitive materials typically made of carbon. In Germany, at Ulm university, the SALVE (Sub-Angström Low Voltage Electron) microscope constructed in partnership with Zeiss and CEOS companies has also recently demonstrated high resolution imaging of the 2D graphene lattice with a primary beam of 20 keV, in the conventional bright field TEM mode [14].

The distribution in shape and size of the incident current within the probe constitutes the first factor to be considered for the definition of the spatial resolution in any of the STEM imaging modes, as it contributes through its convolution with the object function. The spatial resolution can actually be defined using different criteria. One can measure it as its power to discriminate two point sources, or to smooth an abrupt edge. Another useful definition is the diameter of the area containing x% of the primary beam (typically, $x=70$), see [15]. Practically, if we assume that two individual atoms, which are bound with a covalent or an ionic bond, are separated by about 0.2 nm, the introduction of a C_s corrector has dramatically improved the situation: with a standard VG STEM, they could not be resolved, with a corrected focusing optics, they can.

2.2. About the signals of interest generated by the electrons while interacting with the target

While propagating through the specimen, the incident electrons suffer elastic as well as inelastic processes, with some of them inducing secondary emission of electrons and of photons in particular (see for instance [16,17]). When tracking the signature of individual atoms, the specimen is extremely thin, so that single scattering conditions prevail. In this paragraph, we focus on the description of the information carried through these different channels.

2.2.1. Elastic scattering at large angles

This is the most basic process used in STEMs to visualize the specimen. It is due to the Coulomb interaction between the incident electron and the screened atomic nuclei of the sample. The higher the Z number of the atom, the larger the scattering cross-section. As recognized in the first studies by Crewe et al., the elastic cross section follows a power law such as Z^{α}, with α between 1.5 and 2 depending of the angular domain for collecting these electrons. Practically, with a 1 Å diameter probe centered over an atom, the probability for one 100 keV electron to be scattered into a high angle annular dark field detector is of the order of 10^{-4} for low Z ($\sim$10) elements to 10^{-2} for high Z ($\sim$100) elements. This signal is therefore very efficient to visualize heavy atoms on a thin foil made of light elements.

As a matter of fact, the visibility criterion introduced by Crewe and coworkers [1] to support their claim of a first visualization of heavy single atoms, relies on a rough estimate of the signal-to-noise ratio (SNR) in the case of a single U atom on top of a thin carbon foil (typically less than 5 nm thick) for a given primary dose of electrons. As demonstrated and used in several papers (see for instance [18]), the SNR for the detection of a feature of contrast C in an image with an average number of counts per pixel $<n>$ behaves as: SNR$=<n>.C^2$. Consequently, it cannot discriminate atoms of close Z because their relative contrast (C) is too weak. However, with the largely increased primary dose carried in a C_s corrected beam and the associated increase of $<n>$, Krivanek et al. [19] have recently shown an histogram of ADF intensities discriminating individual B, C, N and O atoms within a mono-layer of h-BN incorporating impurities. Two experimental aspects have to be pointed out in this successful experiment, a lower primary voltage which increases scattering cross sections and reduces knock-on beam damage, and a detector of reduced inside angular acceptance for picking more of the electron distribution weakly scattered by such low Z atoms.

2.2.2. EELS core-losses for elemental identification and bonding maps

As a consequence of the limited discriminating power of the HAADF signal, the privileged approach to identify one atom without ambiguity lies in the elemental characteristic core-losses in an EELS spectrum. There exist rather few overlaps in energy between edges to be attributed to different elements, so that the position of the threshold for an edge is a clear hint for a positive identification. Furthermore, the total intensity of an edge after background subtraction is directly connected to the number of atoms through the corresponding cross-section, and the fine structures on the edges are related to the local density of unoccupied electron states, which in the case of individual atoms reflects valence states and local coordination.

In the mid seventies, several studies [20,21] speculated on the ultimate performance in microanalysis potentially achievable by this EELS technique. As an example of their conclusions, Isaacson and Utlaut wrote in 1979 [22]: "It appears that single-atom mapping is within the domain of practicality: it only remains for someone to try to do it"! The major difficulty is due to the fact that the probabilities of exciting given core-shell atoms such as the 1 s level on a carbon atom or the 2p level on a Fe atom are typically two orders of magnitude less than for the acquisition of a HAADF signal on a mid Z atom. This estimation deals with a characteristic signal integrated over a window of 50 eV. When one wants to move one step further, i.e., when the signal of interest is the variation of the fine structures on the EELS signal and the acquisition of bonding maps, the characteristic energy width of the signal of interest is only of 1 eV so that the probability is again nearly 2 orders of magnitude lower.

In their analysis [20], Isaacson and Johnson developed the framework for predicting relevant quantities for microanalysis, such as the minimum mass fraction (MMF), or minimum

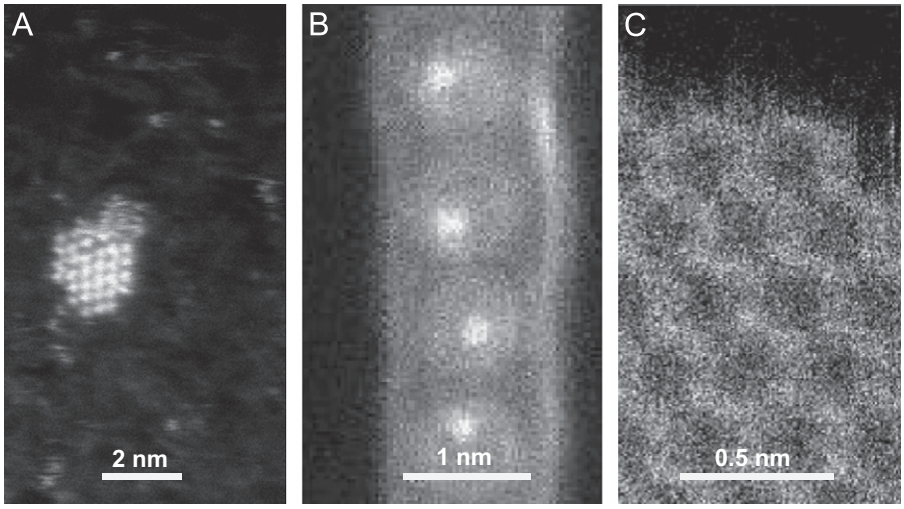

Fig. 2. Gallery of specimens used for STEM-EELS analysis and spectroscopy at the single atom level: (a) mixed Th and Tb clusters (likely oxides) and individual atoms on a thin amorphous layer of carbon; (b) individual lanthanide atoms in endohedral C_{82} fullerene molecules trapped in single-walled CNT; (c) monolayer of C atoms in a graphene sheet. All images are recorded in the HADF mode with a Cs corrector.

concentration C_{min}, under the probe and the minimum detected mass (MDA) or minimum number of atoms N_{min} to be detected within the irradiated volume. Revisiting this approach, Colliex [23] has introduced simple laws: $C_{min} \propto 1/(IT)^{1/2}$ and $N_{min} \propto 1/(JT)^{1/2}$, where I is the probe current, J is the probe current density and T is the counting time, equal to the irradiation time for a parallel EELS (PEELS) detector. Consequently, the smallest detectable concentration depends only on the total intensity of the electron probe, so that it is recommended to use a large and intense probe for detecting small concentrations of an element homogeneously spread throughout the specimen. On the opposite, aiming at N_{min} as low as possible, down to unity, requires increasing the SNR by using highest probe current densities. It can be attained with a high brightness electron source and it does not imply necessarily the smallest probe size and a C_s corrected probe.

Another important parameter limiting the spatial resolution in inelastic signals is associated to the width of the interaction potential at the origin of the scattering event, this effect has been generally designed as the delocalization – r_{in} – (see for instance in [17], chapter 5, p. 347). Several arguments have been developed to estimate it, either in classical or quantum descriptions. In simple terms, it can be retained that r_{in} varies as $v/\Delta E$, where v is the speed of the primary electron and ΔE is the energy loss of interest. Consequently, the degradation in spatial resolution to be attributed to this fundamental physical limit decreases with lower primary voltages and higher energy losses.

2.2.3. Other signals, such as photon emission

Once the specimen has been brought into an excited state, corresponding to the energy-loss suffered by the incident electron, it relaxes via different processes. In the case of an individual atom, the excited state corresponds to the promotion of an electron from an occupied energy level towards an empty one. A major channel for deexcitation lies in the generation of secondary particles, and in particular of photons, of quite variable wavelengths. They can be in the visible (or near visible IR and UV) domain and their spectral analysis constitutes a very useful channel for the identification of electron states. When in the X-ray domain, they have been used for decades as a powerful technique for elemental identification as their spectral analysis provides a pattern of lines which can be unambiguously related to a given type of atom. However, the relatively low value of the fluorescence yield (the probability of generating one photon per primary hole created on an inner atomic level) constitutes a drawback for X-ray emission when compared to EELS to identify a single atom.

2.3. About the detection strategies

The STEM approach for recording the different channels of information produced by electron-matter interactions, derives from those developed by physicists in many domains. It consists in implementing the most efficient detector strategy. The basic idea is to collect through a set of detectors as most as possible of the electrons which have impinged on the specimen and suffered different scattering events, in order not to lose useful information. Consequently, different and complementary signals are collected in parallel for each position of the probe (i.e., for each image pixel) on the specimen successively addressed by the digital scan unit.

One set of detectors consists in annular detectors, the inner and outer angular dimensions of which are set to collect different fractions of the electrons scattered at large angles by elastic events. They are generally made of a combination of scintillators and photomultipliers which are capable of single electron counting.

For the acquisition of the EELS spectrum, a major progress has been the implementation of parallel detection with a multichannel photodiode optically coupled to a scintillator at the exit of the magnetic spectrometer [24]. It has dramatically improved the collection efficiency for the characteristic core-loss edges used for elemental identification. In particular, as it has reduced the required counting time for recording an EELS spectrum of interest, it has opened the field to the spectrum-imaging techniques, first described by Jeanguillaume and Colliex [25]. It consists in acquiring one EELS spectrum covering the spectral domain of interest for each probe position on the specimen, building thus full 3D blocks of data in which two coordinates correspond to positions on the specimen and the third one is an energy loss scale. Altogether, this was the background of the STEM instrument developed for tracking the identification of a single atom: a fully digitized STEM-EELS system, incorporating a most efficient EELS detector (with typically 20 counts/impinging electron) and providing spectrum-images [26].

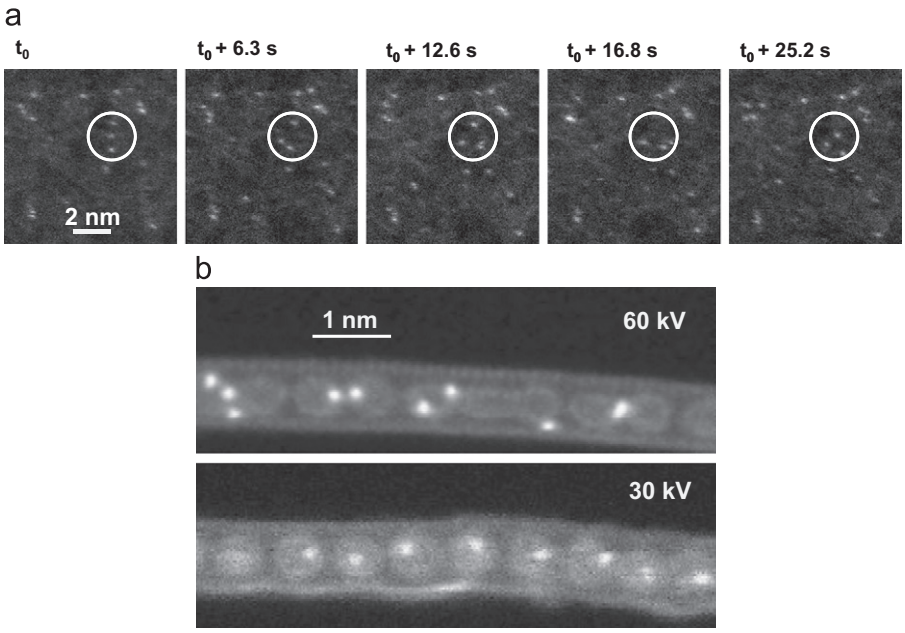

Fig. 3. Examples of dynamic instabilities of atomic specimens: (a) movement of individual atoms monitored by successive HADF images in the Nion UltraSTEM operated at 60 keV; (b) fusion of neighboring peapods induced by 60 keV incident electrons compared to the stability of the structure under primary 30 keV electrons (recorded with the JEOL tripleC STEM).

3. Suitable specimens

Developing the microscope optimized for visualizing and identifying a single atom in terms of signal to noise and of spatial resolution, only constitutes part of the challenge. The other one is to prepare the specimen dedicated to this type of investigation.

3.1. Criteria for selecting the specimens

Since the early studies by the Chicago group, the most widely observed specimen was made of random distributions of heavy atoms on thin carbon foils, produced by a coating with a dilute solution of salts (uranyl acetate or thorium nitrate). For instance, Isaacson et al. have used this type of specimen to realize a detailed study of the adsorption and diffusion of heavy atoms on light element substrates [27]. In our experimental investigation of the ultimate EELS spatial resolution [28], the specimen was a positively stained preparation of DNA molecules spread on a very thin layer of amorphous carbon. The heavy metal atoms used for visualizing the biological structure are concentrated in clusters of nm-size (likely oxide clamps) along the molecules. However, some of them are not involved in the staining, they constitute smaller clusters of sub-nm size made of a few atoms or they stand by themselves (see Fig. 2(a)). The selection of staining agents containing either thorium or uranium atoms, and also those incorporating rare-earth elements, are very attractive. They actually produce high HAADF signals for immediate visualization and localization as well as characteristic signals for elemental identification with a strong cross section (O_{45} for uranides and N_{45} for lanthanides all located in the 100 to 200 eV spectral range).

However, it could be quickly noticed [27] that the specimen does not remain stable under the required electron doses and that the cluster morphologies and positions of individual atoms evolve (see Fig. 3(a)). Consequently, techniques of image duplication and cross correlation techniques have been introduced to evaluate quantitative parameters such as resolution and SNR [29] under these time-varying conditions. As a result of general interest, it was thus shown that for an energy loss of 100 eV and a primary voltage of 100 kV, an upper limit for the extent of the non-local character of the interaction, mentioned above, is about 0.3 to 0.4 nm.

A decade later, a new family of specimens exhibiting a sequence of individual atoms positioned at regular intervals over vacuum has been synthesized [30] and has constituted a quite suitable test object. They are made of Ln (La, Ce, Gd, Er), or eventually Ca, endohedral metallo-fullerenes encapsulated along the core of single-walled carbon nanotubes (see Fig. 2(b)). Practically, they exhibit single atoms with rather high HADF signals and characteristic N_{45} lines, separated typically by one nm and stabilized within a two atom thick carbon layer (the fullerene molecule plus the nanotubular envelop) generating a weak signal in HADF as well as in core-loss maps. They constitute a best approximation for the ideal situation of well-resolved individual atoms self-supported in vacuum.

More recently, graphene (or their equivalent hexagonal BN) single layers have become a favorite specimen for high resolution studies of defects in a perfect 2D atomic thick specimen. The major output of electron microscopy is to identify and resolve point defects, such as substitution and insertion of foreign atoms [19] or on specific sites at the rim of the perfect atomic layers (see Fig. 2(c)).

3.2. Stability under the incident beam

Specimens prepared for recording the signature of individual atoms, are generally made of low *Z* elements and imply rather weak bonds between the atom and its environment. They are quite beam sensitive and can move or degrade under the action of the incident electrons. Knock-on damage is a major aspect of beam damage, occurring by transfer of kinetic energy above a given threshold value. A detailed calculation of knock-on cross sections on carbon and boron nitride nanotubes has been published by Zobelli et al. [31] accounting for anisotropy effects. It concludes that theoretically, the primary voltage for introducing such damage on pure and perfect *C* nanotubes is of the order of 80 kV and of 70 kV for BN ones. It is therefore responsible for limitations in the acquisition of useful data at 100 kV. However, for more refined studies dealing for instance with the interaction

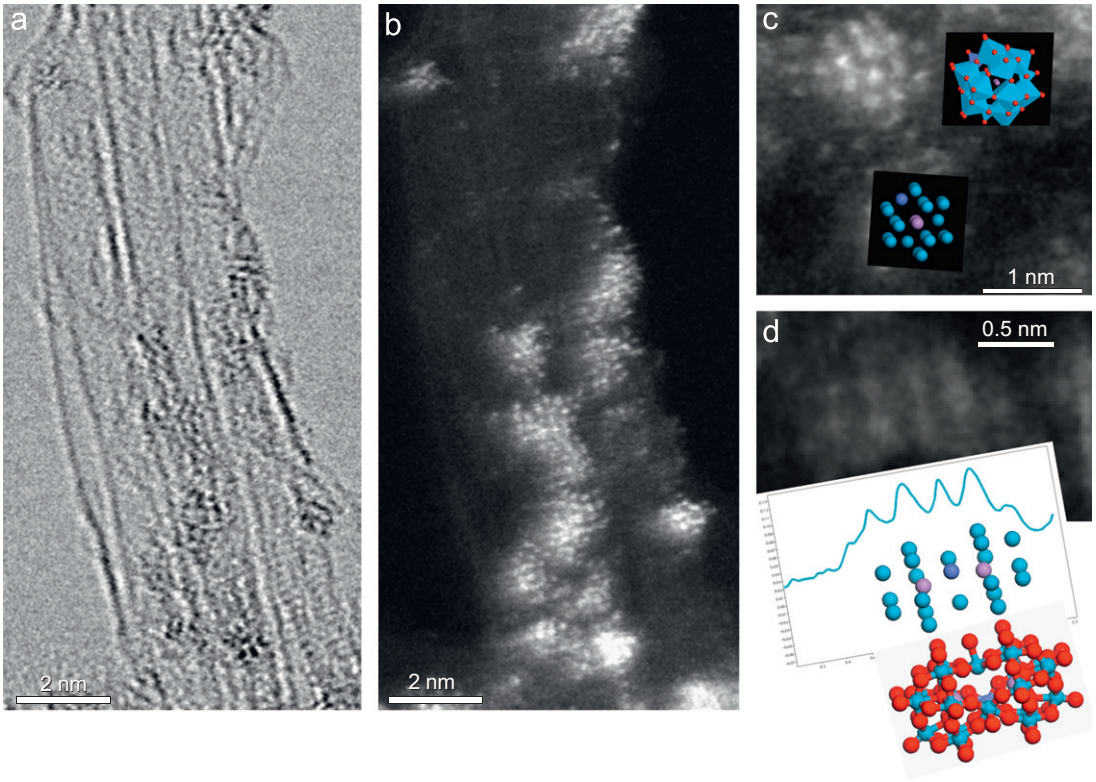

Fig. 4. ((a) and (b)) 60 keV STEM-BF and STEM-DF images of polyoxometalate $As_2W_{20}O_{70}Co(H_2O)$ grafted on SWNTs. (c) STEM-DF of intact POM and two structural models with polyhedron view and with only metallic W and As atoms being visible, (d) STEM-DF of intact POM and contrast profile along the molecules. The 5 contrast peaks correspond to the metallic sequence of 3W, 6W+As, 2W+Co, 6W+As, and 3W atoms and the corresponding atomic models are displayed at the same scale (with and without oxygen atoms). The distances between the two extreme 3W planes are measured at 1.13 nm slightly smaller than the theoretical 1.17 nm expected for this molecule, easily explained by a small tilt of the POM.

of defects with foreign atoms and consequently involving lower binding energies, the threshold voltage for having access to preserved structures without beam induced changes, may be lower. Most recent studies investigating such effects have therefore been conducted at 60 kV and eventually down to 30 and 20 kV.

Therefore, under a 60 keV primary beam, C-SWNT can be imaged with improved stability together with the adsorbed species which they support. For example, BF and HAADF images of tungsten polyoxometalate (POM; $As_2W_{20}O_{70}Co(H_2O)$) grafted on C-SWNTs [32] clearly show the nanotube surface, the POM molecules, clusters of POM but also individual W atoms arising from the degradation of the molecules during the chemical grafting (Fig. 4(a) and (b)). Nevertheless, intact molecules are also evidenced at the surface of the SWNT by resolving the distribution of the heaviest W elements within individual molecules (Fig. 4(c) and (d)).

Furthermore, the advantage of STEM analysis and imaging at lower voltage such as 30 kV has clearly been demonstrated by Suenaga et al. [33]. Many metallofullerene molecules are punctured and coalesce due to beam damage at 60 kV, while they do not show noticeable change and the cage structure is preserved at 30 kV, see Fig. 3(b). As a consequence, building low voltage microscopes preserving atomic level spatial resolution, with the help of C_s (and now of C_c) correctors, is well suited to future successful investigations of individual molecules and atoms.

4. A long way from prediction to success

The quest for capturing the response of an individual atom, beyond seeing it, to the impact of the fine electron probe of a STEM has been pursued over the past four decades since the pioneering work by Albert Crewe and his colleagues at Chicago. In the following, we will summarize the efforts, successes and limitations when using microscopes first without, then with aberration correctors. In the first case, the major barrier to break was that of signal-to-noise, then both barriers set by signal-to-noise and by spatial resolution were broken. In all cases, the physical limitation set by inelastic delocalization constituted part of the challenge.

4.1. Identification of a single atom

Although the identification of a single atom had been predicted in the mid seventies, it took about 25 years before Suenaga et al. reported the success of an element-selective single atom imaging experiment [34]. It was realized with the best STEM instrument available at that time for recording with high efficiency the weak N_{45} signal of the Gd atoms doping fullerene molecules aligned in the core of SWNTs (as displayed in Fig. 2(b)). In this experiment, the Gd atoms are separated by a distance of the order of one nm, so that there is no stringent spatial constraint for resolving them. The authors could quantify the characteristic Gd signal in multiples of a quantity corresponding to a single atom, with a SNR much higher than 3. The spectrum-image technique has been essential in this work for recording about 4000 individual EELS spectra encompassing the characteristic Gd and C edges, each spectrum requiring a 35 ms acquisition time. The major limitation identified in this work was the sensitivity of the specimen to the primary 100 keV electron beam: Gd atoms are missing in some fullerenes and others are aggregated in fused adjacent molecules. This coalescence process is revealed by the increase of the characteristic signal, but with the

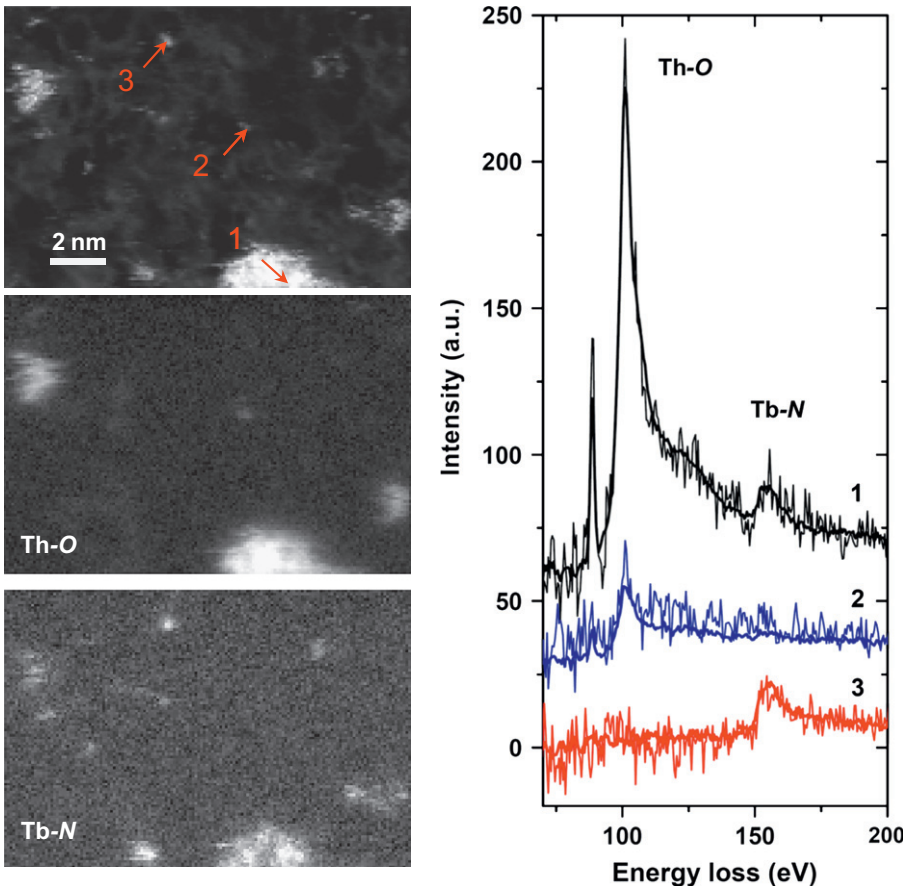

Fig. 5. Spectroscopy and mapping at the single atom level with a Cs corrected Nion UltraSTEM microscope operated at 60 kV using the spectrum-image acquisition and processing mode. Probe step is of 0.1 nm, acquisition time of 5 ms per spectrum. A Principal Component Analysis (PCA) has been performed on the EELS spectra. The investigated area is extracted from the analysis of a DNA filament deposition, stained with 0.1% of Th and 2% of Tb (prepared by S. Baconnais and E. Delain, IGR, Villejuif). The probe diameter is estimated to be of 95 pm.

typical 0.5–0.7 nm diameter of the probe used in these experiments, the individual atoms could not be discriminated.

Several contributions had prepared the way to a clear identification of a single atom. Some of them were all concluded by some assertion of the type: "For the case of small thorium clusters on a thin carbon film, the detection limit with currently available instrumentation is shown to be one atom". This resulted from an extrapolation of quantitative experimental measurements, using parallel detection EELS in the first difference mode, on thorium clusters of smaller and smaller size in [35]. In another study dealing with biological specimens (DNA plasmids and tobacco mosaic virus-TMV-), Leapman and Rizzo [36] have reached a similar conclusion for biologically important elements such as P or Ca. It is also an extrapolation of phosphorus maps using the L_{23} edge, with clear signals corresponding to 3–5 P atoms per pixel. Note that these last experiments were performed with a primary electron energy of 40 keV.

Once aberration-corrected STEM optics have been available, the reduction in probe diameter and the increase of the current carried by small probes have rapidly broadened the possibilities of single atom identification. In a completely different type of specimen, a well crystallized oxide layer ($CaTiO_3$ doped with a small fraction of La atoms), Varela et al. [37] could detect the La M_{45} lines at 840 eV for a single heavy La atom substituted in a Ca column aligned parallel to the electron beam. The signal vanishes nearly completely when the probe is moved on top of the adjacent column separated by about 0.15 nm. In an extended analysis of such data, Varela et al. [38] investigated how one can count impurities substituted on adjacent parallel columns and how accurate simulations are required for upgrading it with confidence to a scale integer by integer.

The issue of single atom identification with core EELS signals can be revisited with a C_s corrected probe of 0.1 nm and at 60 kV. For the first type of specimen introduced in Fig. 2(a), spectra recorded on a single pixel exhibit a very high SNR as demonstrated in Fig. 5. Unprocessed spectra and PCA filtered ones are shown, recorded on the center of a cluster in position 1 (with both Th and Tb edges), at the apex of a single atom visible in the HADF in position 2 (likely a Th atom) and in position 3 (likely a very small cluster made only of Tb atoms). Characteristic maps for the two elements are also displayed, they reveal that the big cluster is of mixed type, mostly made of Th atoms while the isolated atoms can be of either type. The elemental maps confirm that the spatial resolution is degraded with respect to the HADF dark field. This is a confirmation of the importance of the inelastic delocalization parameter mentioned above. In particular, the situation is worst with the Th O edge at 100 eV than with the Tb N edge at 160 eV.

The reduction of primary voltage down to 60 kV and eventually better at 30 or 40 kV, has also been shown to be essential for preventing peapods from massive destruction over the long period required for mapping and identifying atoms of different nature. With the access to the aberration corrected instrument described in [5], Suenaga et al. could progress significantly with respect to the Gd atom identification demonstrated in year 2000. The specimen is now made of peapods doped with various metallofullerene molecules so that single atoms of different nature can be maintained isolated in neighboring cages [39]. As an example, Fig. 6 shows maps of La ($Z=57$) and Er ($Z=68$) atoms

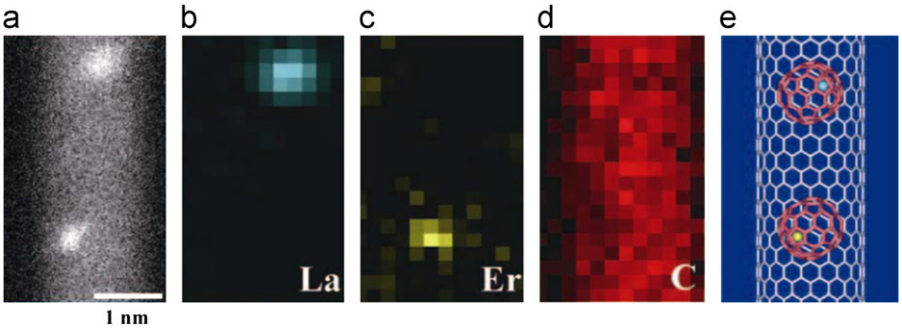

Fig. 6. Element-selective imaging of single La and Er atoms. (a) ADF image of a co-doped peapod with La@C_{82} and Er@C_{82}. Two atoms are visible but the elemental identification is not possible. (b)(c)(d), EELS maps for La (blue), Er (yellow) and carbon (red), respectively. La and Er atoms are clearly visible and discriminated in each EELS chemical map. (e) A model for the peapod structure examined (recorded with the JEOL tripleC STEM). (For interpretation of the references to color in this figure legend, the reader is reffered to the web version of this article.)

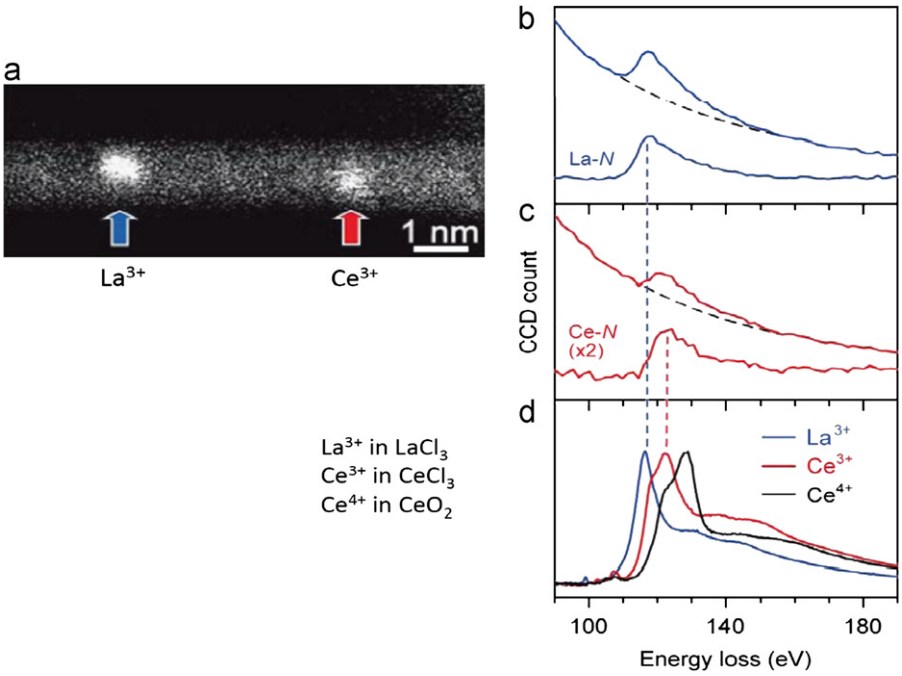

Fig. 7. Single-atom spectroscopy for La and Ce. (a) ADF image of a co-doped peapod with La@C_{82} and Ce@C_{82}. (b)(c) EELS spectra taken from the two atoms indicated by blue and red arrows, respectively, in (a). (d) Reference EELS spectra of La^{3+} (in $LaCl_3$, blue), Ce^{3+} (in $CeCl_3$, red) and Ce^{4+} (in CeO_2, black). The atom (left) in (a) is assigned as La and the atom (right) as Ce in the trivalent state (Ce^{3+}), (recorded with the JEOL tripleC STEM). (For interpretation of the references to color in this figure legend, the reader is referred to the web version of this article.)

in a peapod filled with La@C_{82} and Er@C_{82} molecules. Although one cannot discriminate the La and Er atoms in the HADF image (Fig. 6(a)), the EELS chemical maps clearly identify the La and Er atoms (Fig. 6(b) and (c)) because the absorption edges of the La N45 edge (99 eV) and Er N45 edge (168 eV) are distant enough to construct selective images for both elements. This is a clear demonstration of "atom-by-atom" labeling.

If we now consider mixed peapods doped with both La and Ce ($Z=58$) atoms, the situation is more complex. These atoms have the smallest atomic number difference ($\Delta Z=1$) and a difficulty arises when constructing La and Ce EELS elemental maps. Because the onset energies of the La N_{45} and Ce N_{45} edges are very close (99 and 109 eV, respectively), the absorption edges thoroughly overlap and cannot be separated from each other. In addition, a core level shift for Ce^{3+} (a minor valence state rather than the normal Ce^{4+}) makes the two edges closer. Discriminating the nature of the two atoms in the ADF image (Fig. 7(a)) is only possible by checking the threshold and peak energies in the EELS spectra (Fig. 7(b) and (c)). One can identify that the atom at the left side is La and the other at the right side is Ce by comparing the EELS spectra recorded on individual atoms with reference spectra acquired for La^{3+} (in $LaCl_3$), Ce^{3+} (in $CeCl_3$) and Ce^{4+} (in CeO_2), see Fig. 7(d). Furthermore, the valence state of the Ce atom in Fig. 7(a) is +3 (not +4). This experiment evidences that atomic-resolved EELS techniques can be used to discriminate two individual atoms with an atomic number difference of one. Furthermore, the valence state of a single atom can be determined by means of EELS.

4.2. Bonding of a single atom

The fine structures on EELS core-edges are very rich in information. It has just been demonstrated that they carry the signature of the valence state of an ion. Along this general trend, many applications are now carried on using atomic resolved maps of complex oxide structures (see [38] for a glimpse at a few of them). More generally, the progress of the instrumentation now offers access to a real atom-by-atom spectroscopy, which provides for each single atom located on a 2D array or along a line, a full EELS spectrum with its fine structures [40]. As an example,

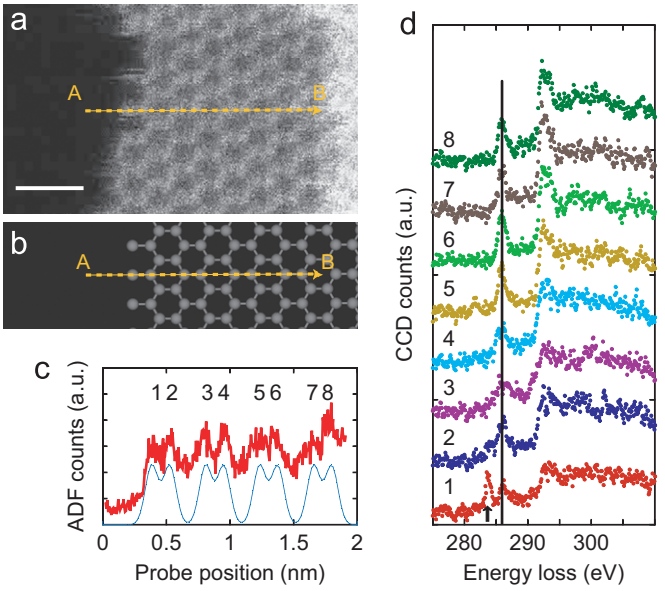

Fig. 8. Atom-by-atom spectroscopy across the Klein edge. (a) ADF image of graphene edge (no image-processing). The dotted arrow indicates where the spectrum-line has been recorded (A to B). (b) An atomic model of the investigated edge. (c) Line-profile of the ADF counts (in red) recorded simultaneously with the spectrum-line. Compared with the simulated ADF counts (blue), the number of each atom is indicated (from 1 to 8). (d) The carbon K-edge ELNES obtained from each atom across the Klein edge. The single coordinated carbon atom (numbered as 1) clearly shows the peak *S* (recorded with the JEOL tripleC STEM). (For interpretation of the references to color in this figure legend, the reader is reffered to the web version of this article.)

Fig. 8 shows a line-spectrum, i.e., a sequence of carbon K edges recorded while scanning the 60 kV incident probe of Å-dimension on top of a graphenic monolayer of carbon atoms, along the dotted line shown in Fig. 8(a). It starts from vacuum and moves onto the bulk and in particular above a protruding atom, namely a Klein edge, with constant steps of ~0.02 nm. For a total number of 100 spectra, the total acquisition time is as small as 50 s. An illustrated model of the investigated structure is shown in Fig. 8(b) where eight carbon atoms are identified along the spectrum-line. Fig. 8(c) shows (in red) the ADF profile which has been simultaneously recorded with the ELNES spectra. There is a good agreement with the simulated profile (in blue) exhibiting eight maxima corresponding to the eight carbon atoms in line. Although the experimental profile is rather scattered due to specimen instability or to a possible inclination of the specimen with respect to the incident electron beam, which could be responsible for a slight asymmetry in the profile of the carbon doublets, it is reasonable to deduce the carbon atomic positions from the line-profile and to extract the ELNES spectra corresponding to each atom. Fig. 8(d) shows the thus obtained ELNES fine structures for the corresponding atoms numbered in Fig. 8(c) (each spectrum actually consists of a sum of 4 individual spectra). Most spectra, in particular from position 5 to 8, display the well known profile for the sp^2 bonded C atoms in the planar hexagonal structure, with a π^* peak at 285 eV and a σ^* one at 292 eV. On top of the protruding C atom (position 1), a pre-peak at 283.6 eV significantly below the bulk π edge is clearly visible.

What is the origin of this peak? In [40], the authors propose to attribute it to a singly coordinated C atom, on the basis of DFT (Density Functional Theory) calculations, including core-hole effects. However, other interpretations can be put forward, such as the presence of hydrogen undetectable with the present techniques. This is clearly a good point to end up this review from the visualization of single atoms opened by Crewe and coworkers about 40 years ago to the atom-by-atom spectroscopy demonstrated in these most recent studies by Suenaga and coworkers. The level of information on individual atoms gained through the local probing by a tiny electron beam is so rich that it obviously deserves more refined theoretical simulations.

5. What is next?

At the end of this journey, it is important to point out that there is still plenty of room for future developments, on the instrumental and technical aspects as well as on the broadening of the applications field.

Considering new perspectives in electron microscopy, the present review has demonstrated the fundamental role of a tiny electron probe and of a suitable detector strategy. The advent of monochromators in or at the exit of the electron guns, allows to select narrow energy widths, down to below 100 meV, for the primary beam, giving access to EELS spectroscopies with significantly improved energy resolution. Time-resolved techniques relying on the use of pulsed laser beams for triggering pulsed electron beams and specimen excitation, have been shown to monitor imaging, diffraction and EELS spectroscopy with time resolution reaching the fs-domain [41]. Obviously, this new 4th dimension (time) has not demonstrated up to now high spatial resolution and single atom sensitivity. But, for sure, the technology is ready for monitoring the dynamics of individual atoms, at many different time scales.

Finally, the spectroscopy of emitted photons can generate complementary signals, either for identifying the nature of atoms in individual columns using the X-ray emission [42,43], or for recording the optical response in the IR–visible–UV domain by cathodoluminescence – CL – [44]. In the first case, atomic resolution in crystalline specimens has been demonstrated using X-ray spectral imaging, with reduced delocalization as compared to EELS core-loss spectral imaging. In the second case, spatial resolution at the nm level has been shown on individual quantum dots but energy resolution in optical spectroscopy is much improved with respect to that accessible in EELS. Recording optical spectra on a single atom has not yet been shown, to our knowledge, but it lies within the realm of practical demonstration in a near future.

Seeing individual atoms, identifying them, measuring their optical spectrum will open, for sure, wide fields of applications yet unforeseen. In CL experiments, the attainable spatial resolution in a "bulk" material depends on various parameters, such as the diffusion length of the e–h pairs and the signal generation volume, see [45] for instance. When the investigated object is of nano-size, as for quantum emitters [44] and the accelerating voltage sufficiently high, the size by itself seems to be the limiting factor. The situation for individual atoms would be a priori still more favorable. Furthermore, when it is a priori known that the distance between the emitting atoms is large (typically > a few nm), useful information, when not limited by S/N considerations, should be accessible. As a matter of fact, individual point defects – nitrogen vacancy complexes in diamond – have recently been singled out [46] both spatially and spectrally in CL maps, indicating that decent S/N for individual atoms is at hand. Let us mention one of the potential cases to be addressed: the labeling of biomolecules with fluorescent labels such as lanthanide chelates or lanthanide doped nanocrystals. La ions are very well suited for EELS identification at the level of the single atom, they offer very rich fluorescent spectra quite sensitive to their local environment. We know how to image molecules at lower primary voltages, at low temperatures for preserving them from dramatic radiation damage. As quoted above concerning the identification of a single atom, "it only remains for someone to try to do it"!

Acknowledgments

The authors thank CNRS and University Paris Sud for their continued support to this research over all the years. They acknowledge the many collaborations which have lead to the different successes described here. In particular, Ondrej Krivanek when at Gatan in the 80s gave us access to parallel EELS acquisition, and when at Nion conceived and built the new Cs corrected generation of STEM which we now can operate at Orsay. Christian Jeanguillaume introduced and made EELS spectrum-imaging a practical method. Noel Bonnet†, who has passed away end of 2011, has contributed a lot to the development of image processing methods in the 1980s and 1990s. Etienne Delain has helped us with the preparation of suitable specimens and introduced us to selected issues in molecular biology. One of us, Kazutomo Suenaga, acknowledges a support from the JST-CREST program. Toshiya Okazaki and Masanori Koshino in AIST are gratefully acknowledged for their cooperation.

References

[1] A.V. Crewe, J. Wall, J. Langmore, Visibility of single atoms, Science 168 (1970) 1338.
[2] J. Wall, J. Langmore, M. Isaacson, A.V. Crewe, Scanning transmission electron microscopy at high resolution, Proceedings of the National academy of Sciences of the United States of America 71 (1974) 1.
[3] A.V. Crewe, M. Isaacson, D. Johnson, A high resolution electron spectrometer for use in transmission scanning electron microscopy, Review of Scientific Instruments 42 (1971) 411.
[4] N. Dellby, N.J. Bacon, P. Hrncirik, M.F. Murfitt, G.S. Skone, Z.S. Szilagyi, O.L. Krivanek, Dedicated STEM for 200 to 40 kV operation, European Physical Journal Applied Physics 54 (2011) 33505.
[5] T. Sasaki, H. Sawada, F. Hosokawa, Y. Kohno, T. Tomita, T. Kanayama, Y. Kondo, K. Kimoto, Y. Sato, K. Suenaga, Performance of low-voltage STEM/TEM with delta corrector and cold field emission gun, Journal of Electron Microscopy 59 (Supplement) (2010) S7.
[6] M. Haider, H. Rose, S. Uhlemann, E. Schwan, B. Kabius, K. Urban, A spherical-aberration-corrected 200 kV transmission electron microscope, Ultramicroscopy 75 (1998) 53.
[7] M. Haider, S. Uhlemann, E. Schwan, H. Rose, B. Kabius, K. Urban, Electron microscopy image enhanced, Nature 392 (1998) 768.
[8] O.L. Krivanek, N. Dellby, A.R. Lupini, Towards sub-Å electron beams, Ultramicroscopy 78 (1999) 1.
[9] O.L. Krivanek, P.D. Nellist, N. Dellby, M.F. Murfitt, Z. Szilagyi, Towards sub-0.5Å electron beams, Ultramicroscopy 96 (2003) 229.
[10] O.L. Krivanek, G.J. Corbin, N. Dellby, B.F. Elston, R.J. Keyse, M.F. Murfitt, C.S. Own, Z.S. Szilagyi, J.W. Woodruff, An electron microscope for the aberration-corrected era, Ultramicroscopy 108 (2008) 179.
[11] O.L. Krivanek, N. Dellby, M.F. Murfitt, M.F. Chisholm, T.J. Penniyook, K. Suenaga, V. Nicolosi, Gentle STEM: ADF imaging and EELS at low primary energies, Ultramicroscopy 110 (2010) 935.
[12] H. Sawada, T. Sasaki, F. Hosokawa, S. Yuasa, M. Terao, M. Kawazoe, T. Nakamichi, T. Kaneyama, Y. Kondo, K. Kimoto, K. Suenaga, Correction of higher-order geometrical aberration by triple 3-fold astigmatism field, Journal of Electron Microscopy 58 (2009) 341.
[13] H. Sawada, T. Sasaki, F. Hosokawa, S. Yuasa, M. Terao, M. Kawazoe, T. Nakamichi, T. Kaneyama, Y. Kondo, K. Kimoto, K. Suenaga, Higher-order aberration corrector for an image-forming system in a transmission electron microscope, Ultramicroscopy 110 (2010) 958.
[14] U. Kaiser, J. Biskupek, J.C. Meyer, J. Leschner, L. Lechner, H. Rose, M. Stöger-Pollach, A.N. Khlobystov, P. hartel, H. Müller, M. Haider, S. Eyhusen, G. Benner, Transmission electron microscopy at 20 kV for imaging and spectroscopy, Ultramicroscopy 111 (2011) 1239.
[15] C. Mory, C. Colliex, J.M. Cowley, Optimum defocus for STEM imaging and microanalysis, Ultramicroscopy 21 (1987) 171.
[16] L. Reimer, 3rd edn., Transmission Electron Microscopy: Physics of Image Formation and Microanalysis, vol. 36, Springer Series in Optical Sciences, 1993 Chapter 5, p. 136.
[17] R.F. Egerton, Electron Energy-Loss Spectroscopy in the Electron Microscope, 2nd edn., Plenum Press, 1996 Chapter 3, p. 131.
[18] C. Colliex, C. Mory, A.L. Olins, D.E. Olins, M. Tencé, Energy filtered STEM imaging of thick biological sections, Journal of Microscopy 153 (1989) 1.
[19] O.L. Krivanek, M.F. Chisholm, V. Nicolosi, T.J. Pennycook, G.J. Corbin, N. Dellby, M.F. Murfitt, C.S. Own, Z.S. Szilagyi, M.P. Oxley, S.T. Pantelides, S.J. Pennycook, Atom-by-atom structural and chemical analysis by annular dark-field electron microscopy, Nature 464 (2010) 571.
[20] M. Isaacson, D. Johnson, The microanalysis of light elements using transmitted energy loss electrons, Ultramicroscopy 1 (1975) 33.
[21] C. Colliex, V.E. Cosslett, R.D. Leapman, P. Trebbia, Contribution of electron energy loss spectroscopy to the development of analytical electron microscopy, Ultramicroscopy 1 (1976) 301.
[22] M. Isaacson, M. Utlaut, 1979, In: Proceedings of the 37th Annual EMSA Meeting, San Antonio, TX, Ed. G.W. Bailey (Claitor's, Baton Rouge, LA), p. 524.
[23] C. Colliex, The impact of EELS in materials science, Microscopy, Microanalysis, Microstructures 2 (1991).
[24] O.L. Krivanek, C.C. Ahn, R.B. Keeney, Parallel detection electron spectrometer using quadrupole lenses, Ultramicroscopy 22 (1987) 103.
[25] C. Jeanguillaume, C. Colliex, Spectrum-image: the next step in EELS digital acquisition and processing, Ultramicroscopy 28 (1989) 252.
[26] M. Tencé, M. Quartuccio, C. Colliex, PEELS compositional profiling and mapping at nanometer spatial resolution, Ultramicroscopy 58 (1995) 42.
[27] M.S. Isaacson, J. Langmore, N.W. Parker, D. Kopf, M. Utlaut, The study of the adsorption and diffusion of heavy atoms on light element substrates by means of the atomic resolution STEM, Ultramicroscopy 1 (1976) 359.
[28] C. Mory, H. Kohl, M. Tencé, C. Colliex, Experimental investigation of the ultimate EELS spatial resolution, Ultramicroscopy 37 (1991) 191.
[29] C. Mory, C. Colliex, Elemental analysis near the single-atom detection level by processing sequences of energy-filtered images, Ultramicroscopy 28 (1989) 339.
[30] K. Hirahara, K. Suenaga, S. Bandow, H. Kato, T. Okazaki, H. Shinohara, S. Iijima, One-dimensional metallofullerene crystal generated inside single-walled carbon nanotubes, Physical Review Letters 85 (2000) 5384.
[31] A. Zobelli, A. Gloter, C.P. Ewels, G. Seifert, C. Colliex, Electron knock-on cross section of carbon and boron nitride nanotubes, Physical Review B 75 (2007) 245402.
[32] G. Charron, A. Giusti, S. Mazerat, P. Mialane, A. Gloter, F. Miserque, B. Keita, L. Nadjo, A. Filoramo, E. Rivière, W. Wernsdorfer, V. Huc, J.-P. Bourgoin, T. Mallah, Assembly of a magnetic polyoxometalate on SWNTs, Nanoscale 2 (2010) 139.
[33] K. Suenaga, Y. Iizumi, T. Okazaki, Single atom spectroscopy with reduced delocalization effect using a 30 kV STEM, European Physical Journal Applied Physics 54 (2011) 33508.
[34] K. Suenaga, M. Tencé, C. Mory, C. Colliex, H. Kato, T. Okazaki, H. Shinohara, K. Hirahara, S. Bandow, S. Iijima, Element-selective single atom imaging, Science 290 (2000) 2280.
[35] O.L. Krivanek, C. Mory, M. Tencé, C. Colliex, EELS quantification near the single-atom detection level, Microscopy, Microanalysis, Microstructures 2 (1991) 257.
[36] R.D. Leapman, N.W. Rizzo, Towards single atom analysis of biological structures, Ultramicroscopy 78 (1999) 251.
[37] M. Varela, A. Lupini, H.M. Christen, N. Dellby, O.L. Krivanek, P.D. Nellist, S.J. Pennycook, Spectroscopic identification of single atoms within a bulk solid, Physical Review Letters 92 (2004) 095502.
[38] M. Varela, J. Gazquez, T.J. Pennycook, C. Magen, M.P. Oxley, S.J. Pennycook, Applications of aberration-corrected scanning transmission electron microscopy and electron energy loss spectroscopy to complex oxide materials, in: S.J. Pennycook, P.D. Nellist (Eds.), Scanning Transmission Electron Microscopy: Imaging and Analysis, Springer, 2011, p. 429.
[39] K. Suenaga, Y. Sato, Z. Liu, H. Kataura, T. Okazaki, K. Kimoto, H. Sawada, T. Sasaki, K. Omoto, T. Tomita, T. Kaneyama, Y. Kondo, Visualizing and identifying single atoms using electron energy-loss spectroscopy with low accelerating voltage, Nature Chemistry 1 (2009) 415.
[40] K. Suenaga, M. Koshino, Atom-by-atom spectroscopy at graphene edge, Nature 468 (2010) 1088.
[41] A.H. Zewail, J.M. Thomas, 4D Electron Microscopy: Imaging in Space and Time, Imperial College Press, London, 2010.
[42] M.-W. Chu, S.C. Liou, C.-P. Chang, F.-S. Choa, C.H. Chen, Emergent chemical mapping at atomic-column resolution by energy-dispersive X-ray spectroscopy in an aberration-corrected electron microscope, Physical Review Letters 104 (2010) 196101.
[43] A.J. d'Alfonso, B. Freitag, D. Klenov, L.J. Allen, Atomic-resolution chemical mapping using energy-dispersive X-ray spectroscopy, Physical Review B 81 (2010) 100101.
[44] L.F. Zagonel, S. Mazzucco, M. Tencé, K. March, R. Bernard, B. Laslier, G. Jacopin, M. Tchernycheva, L. Rigutti, F.H. Julien, R. Songmuang, M. Kociak, Nanometer scale spectral imaging of quantum emitters in nanowires and its correlation to their atomically resolved structure, Nano Letters 11 (2011) 568.
[45] N. Yamamoto, J.C.H. Spence, D. Fathy, Cathodoluminescence and polarization studies from individual dislocations in diamond, Philosophical Magazine B 49 (1984) 609.
[46] L.H.G. Tizei, M. Kociak, Spectrally and Spatially Resolved Cathodoluminescence of Nanodiamonds: Local Variations of the NV0 Emission Properties, Nanotechnology 23 (2012) 175702.